Effects of wintertime polluted aerosol on cloud over the Yangtze River Delta: case study

Chen Xu [a], Junyan Duan [a], Yanyu Wang [a], Yifan Wang [a], Hailin Zhu [a], Xiang Li [a] *, Lingdong Kong [a], Qianshan He [b], Tiantao Cheng [a] *, Jianmin Chen [a]

a. Shanghai Key Laboratory of Atmospheric Particle Pollution and Prevention (LAP[3]), Department of environmental science and engineering, Fudan University, Shanghai 200433, China;

b. Shanghai Meteorological Bureau, Shanghai 200030, China;

* Corresponding authors: Tiantao Cheng, Xiang Li

Tel: (86) 21-6564 3230; fax: (86) 21-6564 2080;

Email: ttcheng@fudan.edu.cn, lixiang@fudan.edu.cn

Abstract

The effects of polluted aerosol on cloud are examined over the Yangtze River Delta (YRD) using three-month satellite data during wintertime from December 2013 to January 2014. The relationships between aerosol properties and cloud parameters are analyzed in detail to clarify the differences of cloud development under varying aerosol and meteorology conditions. Complex relationships between aerosol optical depth (AOD) and cloud droplet radius (CDR), liquid water path (LWP) and cloud optical thickness (COT) exist in four sub-regions. High aerosol loading does not obviously affect the distributions of cloud LWP and COT. In fact, an inhibiting effect of aerosol occurs in coastal area for low-and medium-low clouds, more pronounced in low clouds (<5km) than high clouds. Low aerosol loading plays a positive role in promoting COTs of high- and low-clouds in areas dominated by marine aerosol. The most significant effect presents in valley and coal industry districts for clouds except high-cloud. The smallest values and variations of cloud parameters are observed in dry-polluted area, which suggests that dust aerosol makes little difference on clouds properties. Synoptic conditions also cast strong impacts on cloud distribution, particularly the unstable synoptic condition leads to cloud development at larger horizontal and vertical scales. The ground pollution enhances the amount of low-level cloud coverage even under stable condition. Aerosol plays an important role in cloud evolution for the low layers of troposphere(below 5km) in case of the stable atmosphere in wintertime.

Keywords: Aerosol, Cloud, Pollution, the Yangtze River Delta

1. Introduction

Aerosol is the solid or liquid particles of 0.001-10 microns in diameter suspended in the atmosphere. Aerosol can influence regional and global climates by direct and indirect effects (Ackerman et al., 2000; Forest et al., 2002; Knutti et al., 2002;Anderson et al., 2003; Lohmann and Feichter, 2005; Satheesh et al., 2006), and cause great harm to atmospheric environment and human health (Monks et al., 2009; Pöschl, 2005). Actually, aerosol can act as cloud condensation nuclei (CCN) or ice nuclei (IN) to affect cloud droplet size, number and albedo, as a result, delaying the collision and coalescence in warm clouds (Twomey, 1974). Aerosol also affects precipitation and cloud lifespan, and eventually affect cloud coverage and regional climate (Albrecht, 1989; Rosenfeld, 2000; Ramanathan et al., 2001; Quaas et al., 2004). In the process of cloud formation, aerosol probably influences cloud physical characteristics, such as cloud thickness and cloud amounts (Hansen et al., 1997).

The Yangtze River Delta (YRD) is a fast growing and densely populated area in East China, hence experiencing relatively high aerosol loadings for decades because of large amounts of black carbon and sulfate emissions (Wolf and Hidy, 1997; Streets et al., 2001;Xu et al., 2003; Bond et al., 2004; Lu et al., 2010). Due to human activities and special geographies, this region suffers a lot from natural and anthropogenic aerosols. In addition to industrial aerosols caused by human activities, the other major types are marine aerosols from sea surface brought by winds and dust aerosols transported occasionally from deserts in northern China mostly in winter and spring (Jin and Shepherd, 2008). All these factors may result in a more complex aerosol-cloud-precipitation interaction over this region.

In recent years, we have paid increasing attention to aerosol and its radiative effects in the YRD district (Xia et al., 2007; Liu et al., 2012). For instance, He et al. (2012) explored that a notable increase of annual mean aerosol optical depth (AOD) takes place during 2000-2007, with a maximum in summer dominated by fine particles and a minimum in winter controlled by coarse mode particles mostly. Other studies have focused on aerosol indirect effect (AIE) (the process of aerosol microphysical effects on clouds) and attempt to assess the impact of aerosol on precipitation in Eastern China. For example, Leng et al. (2014) pointed out that aerosol is more active in hazy days in Shanghai. Tang et al. (2014) analyzed the variability of cloud properties induced by aerosol over East China from satellite data, and compared land with ocean areas to understand AIE discrepancy under different meteorological conditions. Menon et al. (2002) proposed that the increasing precipitation in southeastern China as well as the decreasing precipitation in northeastern China led by anthropogenic aerosol are likely attributable to the absorption radiation by AOD distribution. Zhao et al. (2006) examined the feedback of precipitation and aerosol over the Eastern and Central China for the last 40 years, and revealed that precipitation has significantly decreased as a result of atmospheric visibility reduction. Despite of the above-mentioned studies, up to now, the influence of polluted aerosol on cloud and precipitation over different underlying surfaces along the YRD is not intensively examined.

In the winter of 2013, China was extensively hit by haze, which was characterized by long-term durability, wider influence and severer polluted features. In the YRD, haze occurred persistently at the wintertime from December 2013 to February 2014. In order to understand the formation of haze, Leng et al. (2015) analyzed the synoptic situation, boundary layer and pollutants of haze that happened in December 2013, and Hu et al. (2016) profiled the chemical characteristics of single particle sampled in Shanghai. Kong et al. (2015) observed the variation of polycyclic aromatic hydrocarbons in $PM_{2.5}$ during haze periods around the 2014 Chinese Spring Festival in Nanjing. More efforts are needed to focus on the relationship between aerosol types and macro-/micro-physical properties of clouds under different atmospheric conditions.

Satellite measurements of aerosols, called aerosol optical thickness, are based on the fact that the particles change the way to reflect and absorb visible and infrared light. The hygroscopic property of aerosol will change the values of AODs in case of the same aerosols density. For example, a higher relative humidity increases the AOD due to more water uptake by the particles. Many studies have worked on the relationship between AOD and aerosol concentration. For instance, G. Myhre et al. (2007) point out that the increase in AOD is not mainly caused by the hygroscopic growth, for in many areas, the Angstrom exponent increases as AOD from MODIS increases. Thus, we use AOD to represent of aerosol loading.

This paper presents the spatio-temporal variations of aerosol and clouds over the YRD region from December 2013 to February 2014based on satellite data retrievals and the method used by Costantino et al. (2013). The aim is to provide insights into the influence of aerosol on cloud microphysical properties under highly polluted conditions. In other words, whether the high aerosol loading can induce different effects on cloud development. The results are helpful to in-depth understanding of aerosol indirect effects in Asian fast-growing areas.

2. Data and methods

Clouds and Earth's Radiant Energy System(CERES), part of the NASA's Earth Observing System (EOS), is an instrument aboard Aqua satellite to measure the upwelling short- and long-wave radiations with a horizontal resolution about 20×20 km^2 (Wielicki et al., 1996; Loeb and Manalo-Smith, 2005). In this study, the clouds and aerosol parameters of CERES-SYN1deg, retrieved from Edition 3A 3-hour data from satellites of Terra and Aqua, were used for the YRD domain (26.5-35.5°N, 115.5-122.5°E) between December 2013 and February 2014. Cloud properties, including cloud liquid water path (LWP), cloud effective droplet radius (CDR), cloud optical thickness (COT), cloud top pressure (CTP) and cloud fraction (CLF), were retrieved from the 3.7 μm (mid-IR) channel with the horizontal resolution of 1°×1°(Minnis et al., 2004). The daily average was computed based on the 3-hour data in corresponding to the date from the SYN1deg-3hour products (also for monthly average). On the basis of three-month mean AODs at 0.55μm and underlying surface conditions, the YRD was divided into four sub-regions (Fig.1). If more than 2/3 space of the grid fell into a certain sub-region, this grid was considered as one part of the sub-region.

The CERES-SYN retrieval includes MODIS-derived cloud and aerosol properties (Minnis et al., 2004; Remer et al., 2005) and geostationary-derived cloud properties. It uses 3-hour cloud property data from geostationary (GEO) imagers for modelling more accurately the variability of CERES observations. Computations use MODIS and geostationary satellite cloud properties along with atmospheric profiles provided by the Global Modeling and Assimilation Office (GMAO). Furthermore, the CDR and COT of MOD04 are generally smaller than those of MOD06 products (Minnis et al., 2004; Platnick et al., 2003) because the MODIS algorithm tends to classify very thick aerosol layers as clouds and non-aerosols (Remer et al., 2006). Thus, the total AOD is probably underestimated by MODIS. Overall, the properties of cloud and aerosol are better to be retrived from the CERES-SYN (Jones et al., 2009).

MODIS products are derived from cloud-free data at 500m spatial resolution and then aggregated to a 10 km footprint (20×20 pixels) to generate the MODIS level2 aerosol product (MOD04). The fine mode fraction (FMF) of aerosol at 0.55 μm was used to determine the effect of aerosol types on cloud properties. In this study, the simple method, which was utilized by Barnaba and Gobbi (2004) based on the combination of AOD and FMF, was implemented to separate aerosol types. This method defines aerosol as marine type with AOD< 0.3 and FMF< 0.8, dust with AOD> 0.3 and FMF< 0.7, and continental type with AOD< 0.3 and FMF > 0.8 or AOD> 0.3 and FMF > 0.7. By the way, aerosol type pixels were created following the resolution of CERES products.

The aerosol and cloud products were retrieved by the CALIPSO lidar instrument, which provided height-resolved information globally since 2006, including the layer fraction of aerosol and cloud and aerosol vertical feature mask (Winker et al., 2009, 2010). In order to examine atmospheric stability, surface lifted index (SLI) and sea level pressure (SLP) from the National Center for Environmental Prediction (NCEP) Reanalysis (Kalnay et al., 1996) were used. The frequency of precipitation was calculated by precipitation rate from reanalysis data obtained.

The Hybrid Single Particle Lagrangian Integrated Trajectory (HYSPLIT) model (Draxler and Rolph 2003; Rolph 2003; www.arl.noaa.gov/ready.html) was used to calculate 72-h air mass forward and backward trajectories every six hours at 9key sites in the YRD. The meteorological data input is from the FNL data set, reprocessed from the final analysis data of NOAA's NCEP by Air Resources Laboratory. Additionally, the data of $PM_{2.5}$concentration came from the on-line monitoring and analysis platform of air quality in China (http://www.aqistudy.cn/).

We collected all the information about the data sources, which we used in this study, to make table1.

3. Results and discussion

3.1Aerosol spatial variation

The terrain characteristics will easily influence the transport of pollution and affect the aerosol characteristics. Figure 1 displays the spatial distribution of 3-h mean AODs over the YRD region from December 2013 to February 2014. AODs range in 0.3-0.9, lower than the annual average (0.5-1.3) (Kourtidis et al., 2015), and show significant distinction due to different surface conditions from north to south. High AODs almost scatter in plains and valleys, particularly at the densely populated and industrialized locations, while low AODs are mainly distributed in hills and mountains. AODs higher than 0.7 are concentrated in the north of the YRD, the central and northern parts of Jiangsu Province and the northern part of Anhui Province, traditional agricultural areas, here which are defined as sub-region A. Furthermore, high AODs of 0.5-0.7 are found in

Shanghai and the northeastern part of Zhejiang Province, typical urban industrial areas, named as sub-region B. The Yangtze River valley in Anhui Province, surrounded by Dabie and Tianmu mountains, is categorized into sub-region C. The Tianmu and Dabie Mountain hinder the transport of surface contaminants away from their source regions, whilst also preventing long-distance transportation of dust aerosol from the north and marine aerosol from the east. AODs lower than 0.5 are observed in mountainous areas throughout the south and west parts of Zhejiang province and the Mount Huang in Anhui province, referred to as sub-region D. For hilly areas with trees (region D), the surface of land has different properties from others, and as a result, it may greatly effect aerosol radiation and the progress of hygroscopic growth (e.g. due to humidity levels enhanced by the trees, new particles' activation).

The 3-month mean AODs are 0.76, 0.62, 0.57, and 0.44 in the sub-region A, B, C, and D, respectively. This feature of aerosol spatial distribution is in accordance with the result concluded by Tan et al. (2015), using 10-year data, that aerosol concentration is higher in north and lower in south, whereas FMF is just opposite to AOD.

The effect of hygroscopic growth depends on what is the dominating aerosol type. According to AOD~FMF classification method (Barnaba and Gobbi,2004), aerosols of the sub-region A are probably categorized into marine, dust and continental types, mainly generated from local urban/industrial emissions and biomass burning. Also, this sub-region is vulnerable to dust blowing from the North China (Fu et al.,2014). In the sub-region B, besides fine mode particles from urban/industrial emissions, coarse mode particulate pollutants have marine aerosols brought by northeastern airflows and dust floating long distance from the north. The large aerosol loading of the Jiaozhou Bay is probably attributed to coarse mode particles due to the humidity swelling of sea salt (Xin et al., 2007). A plenty of construction and industrial activities also contribute numerous dust-like particles to the atmosphere (He et al., 2012). Similar with the aerosol types in the sub-region B, the sub-region C is home to more than one million people, numerous copper-melting industry and coalmines, which are the major sources of local emissions. The sub-region D is dominated by continental and marine aerosols, most of which can be easily detected close to their sources (He et al., 2012). Overall, dust and anthropogenic pollutants often influence the columnar optical properties of aerosol in all parts of northern the YRD. The physical interactions between aerosol and cloud are distinct depending on the aerosol type, which is linked to the regions/terrain characteristics.

3.2 Aerosol and cloud properties

3.2.1 Cloud optical thickness (COT)

Figure 2 shows the distribution of COTs varying with AODs, which are averaged over every constant bin AOD (0.02) from 0.2 to 1. Clearly, COTs are notably uni-modal in the sub-region B, C and D, and almost reach to maximum at AODs of 0.6-0.74. The peaks of COTs are close to 17 in the sub-region C, D and smaller 15 in the sub-region B. A possible reason is that clouds turn thicker in mountainous areas (e.g. sub-region C and D) as a result of new particles' activation (Bangert et al., 2011).In contrast, COTs ascend slowly, and multi-modal peaks appear in the sub-region A, such as COTs 7.1, 8.4in corresponding to AODs at 0.44 and 0.88, respectively.

In the sub-region A, COTs grow as aerosols increase, and particularly COTs of the clouds below 4.6km is correlated with AODs below 0.6 (Table S1). COTs and AODs are positive-correlated at low-level AODs (<0.6) in the sub-region B, C and D and negative-correlated at high-level AODs (0.6-1.0). In the sub-region B, COTs are greatly sensitive to AODs, and COTs of all height-type clouds are affected equally by AODs at low-level. As for high-clouds, the inhibiting effect of aerosol on COTs is more outstanding (R^2=0.47) than the promoting effect. In the sub-region C, except for high-clouds, the influence of low-level AODs on COTs of other type clouds is relatively stronger than that in the sub-region B, while high-level AODs are less influential in the sub-region B than the sub-region C and cast no evident impacts on high-clouds. In the sub-region D, COTs and AODs show a significant positive correlativity at low-level AODs, for example, a steep slope (3.58) appears in high-clouds. Generally, COT links closely with AOD, in particular of low- and medium-low clouds in the sub-region A, low- and high-clouds in the sub-region B and D, and other types except high-clouds in the sub-region C.

3.2.2 Cloud liquid water path (LWP)

Kourtid is et al. (2015) point out that the impact of AODs on cloud cover would greatly overestimated unless water vapor is considered in the YRD, where AODs and water vapor have similar seasonal variations. In addition, recent studies have focused on the possible impacts of meteorological parameters on AOD–COT relationships, such as water vapor (Ten Hoeve et al., 2011) and relative humidity (Koren et al., 2010; Grandey et al., 2013).

Water vapor influence is discussed using LWPs averaged over a constantbin of AODs (Figure 3). The relationship of LWP-AOD is somewhat similar to that of COT-AOD (Figure 2), and AODs of 0.6-0.74 correspond to peak LWPs in the sub-region B, C and D. In the sub-region C, LWPs rise up about 14 times as AODs increase from 0.22 to 0.66, which is the largest increase among these sub-regions. Otherwise, in the sub-region A, although LWPs grow smoothly with AODs on the whole, no distinct peaks are detected, and the amount of cloud water increases by 425% as AODs increase from 0.2 to 0.96. The growth rate of LWPs in the sub-region A is similar to that of the sub-region B, but the promoting effects of AOD zones are quite different between them (0.2-1 vs 0.2-0.6). This discrepancy is responsible for a large amount of non-hygroscopic aerosols in the sub-region A (Liu and Wang, 2010).

Generally, LWPs increase with AODs when AODs are at low levels in the four sub-regions. LWPs and AODs are negative-correlated at high-level AODs in the sub-region B, C and D, but weakly positive- correlated in the sub-region A. Specifically, in the sub-region A, the promotion of aerosol positive effect slows down with cloud height growing and AOD increasing. Although aerosol plays equal roles in all height-type clouds in the sub-region B, the best-fit slopes at high-level AODs are twice as large as those at low-level AODs, and correlation coefficients for the clouds below 4.6km are larger than clouds in higher layers (Table S1). In other words, for each level of clouds, LWPs increase slowly (AOD<0.6) but decrease sharply (AOD>0.6) with AODs growing. Opposite to the sub-region B, the promoting effect of AOD on LWP in the sub-region C at low AODs is marked, while the inhibiting effect is not significant at high AODs (Table S1). In addition, the promoting effect of low clouds in the sub-region C is most outstanding. In the sub-region D, the pronounced effect of AOD on LWP mainly works on low- and high-clouds at low-level AODs (Table S1). Particularly, the best-fit slope of high-clouds, such as 2.53 at low-level AODs and -3.46 at high-level AODs, is much higher than that of other height-type clouds.

Many studies have also displayed the correlation of LWP and AOD in other regions of the world. For instance, a report over Pakistan (Alam et al., 2010), where aerosol is dominated by coarse particles, is similar to our results of the sub-region A, where positive correlations of LWP-AOD are found mainly due to their common seasonal patterns. LWP plays an important role in AIE (L'Ecuyer et al., 2009), and findings confirm that high-aerosol conditions tend to decrease LWP, and the magnitude of LWP reduction is greater in the unstable environment of non-precipitating clouds (Lebsock et al., 2008). Moreover, the fact that increasing LWP is not systematically associated with increasing AOD (Fig.3) indicates there is no definite relationship between AOD and LWP.

3.2.3 Cloud droplet radius(CDR)

Fig.4 presents mean CDRs averaged over a constantbin (0.02) of AODs. Basically, CDRs vary between 9.5μm and 11μm in all 4 sub-regions. For the sub-region A, two sections indicate weak positive correlation between CDR and AOD. For the sub-region B, however, it is of negative correlation for these two sections. As for the sub-region C and D, CDRs have a similar pattern that it decreases as AOD increases at low-level AODs and constantly increases at high-level AODs. Therefore, CDRs show an insignificant dependence on AODs (Table S1).

The non-monotonic responses of cloud properties to aerosol perturbations are shown in Figs 2-4. At low AOD (below 0.4), increases in cloud cover are indicative of physical aerosol-cloud interactions. At larger AOD (0.4~0.6), the increasing in cloud cover can be explained by larger hygroscopic growth near clouds (G. Myhre et al., 2007). In this range

(0~0.6), the addition of aerosol causes a decrease in drop size (CDR), precipitation is suppressed, and clouds develop further (increasing of COT) before raining out and last longer in the more developed stage, thus increasing the average LWP (Albrecht et al., 1989; Ferek et al., 2000).

When AOD grows larger than 0.6, the cloud development is reduced, probably due to that aerosols shade the surface. The reducing surface heating and evapotranspiration make LWP reduced (Koren et al., 2004). On the other hand, absorbing aerosols (such as smoke or dust) can heat the upper levels of the troposphere, which in combination with surface shading stabilizes the atmospheric column and reduces cloud development (Koren et al., 2004,2005; Taubman et al., 2004; Ackerman et al., 2000). As an increase in CCN leads to smaller droplets, evaporation around the sides and top of clouds due to mixing will become more effective at reducing the LWP (Koren et al., 2004; Burnet et al., 2007). Moreover, meteorology effects, such as high-pressure systems, can inhibit convective activity, simultaneously reducing cloudiness while aerosols stay in the source region (Sinclair et al., 2010).

Compared to Wang et al. (2014) which studied over YRD during summer time, the different results probably come from the different characters of meteorological conditions in winter and summer. In winter being relatively static, higher aerosol loading and lower humidity. Also, the wind direction of monsoon is different from summer. It will cause differences in aerosol sources advected into/away from the region, thus influence the aerosols and their effects on cloud. As a whole, CDR shows little exponential dependence on AOD, consequently, simply the exponential presentation is difficult to entirely reflect their complex relationship.

We perform former analyses (section 3.2.1, 3.2.2) on four sub-regions (A-D) that are located close to each other. We consider the meteorological conditions are similar between them. In order to understand AOD-CDR, in this part, variables of cloud height and cloud water content are controlled to evaluate their potentials in different height-type clouds by correlation coefficients of cloud parameters (e.g. CDR, LWP, COT) (Table S1). Firstly, it is notable that a considerable portion of relatively high correlation coefficients mostly occurs in low clouds. Figure 5 shows total cloud and aerosol occurrence frequencies below 10km over the entire YRD. The cloud frequency is multi-modal, ranging from 93% around 1km to 26% around 10km, among which most exceeding 50% obviously occur at the low (< 3km) and high (6-9km) layers. As for aerosol layer fraction, it turns out high frequency occurs below 3.6km above sea level, maximum around 1.2km, and the frequency decreases to zero with increasing heights. Overall, both of cloud and aerosol most frequently appear below 3km, indicating that low-cloud (altitude from the surface to 2.8km) plays an important role in AIE within every sub-region. Thereby, we use 3-h average data of low-cloud from CERES in the following analyses.

Water vapor (WV) has a great effect on CDR. Yuan et al. (2008) summarize that 70% of variability between AOD and CDR is due to changes of atmospheric water content. Moreover, statistics suggests that WV has an evidently stronger impact on cloud cover than AOD over the YRD (Kourtidis et al., 2015). Therefore, we introduce LWP and divide it into six grades for analysis of CDR changes with AOD. In Figure 6, CDRs present different tendencies as AOD changes at different levels of cloud water content. When cloud water content is low (i.e. thin cloud, LWP<50 g/m^2), CDRs increase gradually with AODs. The CDRs in the sub-region A and B increase with AODs synchronously at LWPs of 50 -100, but decrease in the sub-region C and D. Overall， it is indicated that in a mountainous area full of water vapors, the inhibiting effect appears as the aerosol loading increases. When LWP is growing, however, the trend of CDR changes with AODs turns ambiguous.

Meanwhile, some of CDRs show clearly decreasing tendency with LWPs at constant AODs under LWP <200 g/m^2, such as higher AODs (AOD>0.6) in the sub-region D and medium aerosol loading (0.4<AOD<0.6) in the sub-region B. Conversely, for LWP >200 g/m^2, there are no obvious changes with growing LWPs because of limited data. The increasing tendency has been observed in Amazon because of difference meteorological and biosphere conditions (Yu et al., 2007; Michibata et al., 2014).

In this study, we use AOD/LWP to reflect the proportion of aerosol and water content. Figure 7 shows COTs and CDRs averaged over a constant bin (0.1) of AOD/LWP in log-log scale, in which AODs are adjusted to LWPs in same magnitude. COTs decrease with AOD/LWP, while CDRs increase with it in all sub-regions. However, the ranges of COT, CDR, and AOD/LWP values are changeable indifferent sub-regions. In the sub-region A, AOD/LWP maximum (15) is larger than that in other sub-regions, indicating a polluted-dry condition. Correspondingly, COTs decrease from 22.8 toward 0.6 with AOD/LWP and shows a strong correlation. Nevertheless, the weakest tendency (-0.84) indicates that the inhibiting effect on COTs is not as strong as other sub-regions. For the clear-wet sub-region D, COTs are larger than that in the sub-region A at same AOD/LWP values. Also, CDRs vary between 9 and 11, showing a weak dependence on AOD/LWP (Figure 7). Many studies have revealed other factors on CDR variation, such as functions of different aerosol components and cloud physical dynamics (Sardina et al., 2015; Chen et al., 2016).

Furthermore, the relationship between aerosol and precipitation is complex as well. The increase of aerosol may reduce CDR, thus, precipitation will be inhibited under dry conditions. For humid regions or seasons, however, the more particles, the more frequently it is going to rain. Therefore, factors of seasons and locations cannot be neglected.

Obviously, precipitation is seasonally and regionally different under various aerosol loadings. Thus, in the research, we divide the YRD into 4 sub-regions as aforementioned during wintertime, and *a* is defined as a slight pollution status (AOD < 0.5) and *b* as a severe pollution status (AOD > 0.5) (Figure 8). If it is severely polluted in the sub-region A, it rains much more frequently, whereas the frequency of precipitation does not differ too much in the sub-region B and C in terms of different pollution levels. Furthermore, it rains much more heavily in a more severely polluted situation, illustrating that aerosols present the promoting effect on precipitation in the north and central YDR. In an area of severe pollution, the sub-region A enjoys a large proportion of high AODs, explaining the reason of particularly high precipitation frequency. In converse, both frequency and amounts of precipitation under the condition of low AODs are greater than those under the condition of high AODs in the sub-region D, presenting a negative effect of AODs on precipitation. The discrepancy between the sub-region A and D can possibly be owed to different dominant aerosol types, featuring different conversion rate (from cloud water to rainwater) (Sorooshian et al., 2013). The amount of precipitation increases slowly at low CDR of 10-15μm but rapidly at higher values of 15-25μm (Michibata et al., 2014).Since there are few CDRs of high values in the study, the low frequency of big rain becomes explanatory. On the whole, the result is in agreement with Sorooshian et al. (2009), who believe that clouds with low LWP (<500 g/m^2) generate little rain and are not strongly susceptible due to aerosol.

3.2.4 Cloud fraction (CLF)

Cloud parameter of cloud top pressure (CTP) can roughly estimate cloud vertical development. Its role in AOD-CLF interactions has been investigated in previous studies in eastern Asia (Alam et al., 2014; Wang et al., 2014). Moreover, the hygroscopicity of aerosols and meteorological/climatic conditions matters a lot in aerosol–cloud interactions as well (Gryspeerdt et al., 2014). In this study, the AODs dominantly drive the variation of CTP over all the sub-regions, irrespective of the pressure system and water amount (Fig.9 and 10).

Figure 9 shows scatter plot of daily averaged CLF and CTP in four sub-regions at different AODs. CERES daily product data is also sorted into five categories based on AODs at constant interval of 0.2. We draw two trend lines of different aerosol loadings, the yellow one is on subset 0-0.3 and the blue one is on subset 0.8-1. Notably, in the sub-region A and C, the cloud coverage under the condition of high-level AODs are generally larger than that under the condition of low-level AODs. There often exist positive relationships between AOD and CLF even considering WV and synoptic variability (Kourtidis et.al, 2015). Compared with the sub-region A and C, the lower AODs of the sub-region B and D not only have more remarkably positive effects on cloud evolvement, but also possess lager cloud fraction if CTP is less than 700hPa.

Meanwhile, Figure 10 shows CTPs have small differences with AODs among four sub-regions. CLF-CTP under the condition of different AODs is almost cumulatively distributed in one line in the sub-region A, as well as in the sub-region D when the CLF <40%. With regard to the sub-region B, C and D (CLF >40%), high-level AODs are not always associated with small cloud top pressure, suggesting that aerosol-cloud interaction do not lead to the variations of CTP. The possible reasons is that aerosols influence horizontal extension of clouds rather than the vertical distribution (Costantino et al., 2013).

3.2.5 Aerosol types and low clouds

In fact, most of aerosol particles float in the low atmosphere of stagnant conditions during wintertime. To explore relationships between cloud parameters and aerosol types (table 2), we analyze low clouds due to the fact that ample amounts of clouds appear at low altitudes as previously described (Jones et al., 2009). This is a simple consequence of transportation from north by prevailing northern wind in winter over the YRD. As a result, the air mainly saturated with burning fossil fuels and the quality of air is deteriorated. At the same time, partial areas of the YRD are affected by air mass flowing from the highly polluted areas in the Sichuan Basin.

Although dust accounts for a large portion of AOD, marine and continental aerosols make notable effects on COT and LWP in all sub-regions except sub-region A. It is mainly because that, as a kind of poorly hygroscopic aerosols, dust is less likely to be mixed with water vapor and become CCN. Marine aerosols, comprising both organic and inorganic components from primary and secondary sources, have equal impacts on COT and LWP in the sub-region C and D, and furthermore, thicken the clouds. Nevertheless, dust aerosols just have slight impacts on COT and LWP in the sub-region A. Probably, dust particles can be coated with hygroscopic material (i.e. sulfate) in polluted regions, greatly increasing their ability to act as effective CCN (Satheesh et al., 2006; Karydis et al. 2011).

The correlation coefficients, as for CDR, between different aerosol types are close. It is worth noting that negative values of K (best-fit slope) only appear in marine aerosols of the sub-region B and continental aerosols of the sub-region A, B and D. In other words, CDRs decrease along with increasing marine/continental aerosols in the sub-region B and continental aerosol in the sub-region A and D. Additionally, small values of correlation coefficient (R^2) demonstrate that precise analysis can hardly be done if only aerosol types are taken into consideration.

3.3Polluted aerosol and clouds development

Regarding the problem of aerosol and cloud data matching, we add a case study that attempts to match the observed aerosols by satellite to the same source influencing clouds over a series of days. Figure.11 shows the daily average of AODs from 26th January to 8th February, covering both the growing and mitigating process of one pollution event over the YRD region. High AODs mainly scatter in a large domain, involving Shanghai, Anhui Province, northeastern Jiangxi Province, southern and western Jiangsu Province, and northwestern Zhejiang Province on 27th January. Since then, the polluted areas gradually reduce to Shanghai and Jiangsu Province until 2nd February. Obviously, AODs increase from 27th January to 1st February in the north of Jiangsu Province, but decrease from 2nd to 8th February. The traditional Chinese New Year is just within this period.

In order to understand aerosol and cloud vertical distributions during the above mentioned period, frequency profiles of aerosol and cloud calculated by layer fraction from CALIPSO daily data is drawn below 10 km in the region of (31-36°E, 117-122°N). As shown in Figure.12, where four days are chosen for case study and the data of aerosol and cloud layers comes from CALIPSO. It displays that aerosol reaches high frequency (>70%) between the height of 1.2 and 3km on 1st February (Brown line). Meanwhile, cloud layers develop from relatively low occurrence frequency (<60%) below height of 1km to high frequency (the maximum reaches 100%) between the height of 1.2 and 3 km. With the major decline of aerosol at the same altitude on 2nd and 3rd February, clouds occurrence frequency clearly deceases by nearly 30% at the height of 2.5km on 3

February. Furthermore, it is noticed that the peaks of aerosol occurrence frequency arise at higher altitudes, around 4.8km and 6.5km on 3 February as well as 5.6 to 7km on 4 February. Correspondingly, the clouds develop in the vertical.

The daily averages of surface lifted index (SLI), sea level pressure (SLP) and $PM_{2.5}$ concentrations are shown in Figure.13. SLI, calculated by temperature at surface and 500hPa, is applied to indicate the stability status of atmosphere. The time series of SLI variation display a sharp increase from 2.6 to 26.5 degK on 3and 4 February. In addition, the SLP>1008hPa represents the core of high-pressure systems and ascending motions of air. The synoptic system with the growing of lower SLP proves that the air mass ascends in these days. The concentration of $PM_{2.5,}$ sharply declining from 288 $\mu g/m^3$ to 30.5 $\mu g/m^3$, is coincident with air mass updrafts and horizontal transmission.

In addition, to identify the movement path and vertical distribution of aerosol and cloud layers, the air mass forward trajectories matrix from NOAA's HYSPLIT model are shown in Figure.14a, beginning on 2^{nd} February and at 150m height. Most of these forward trajectories show that aerosols are transmitted to southwest at first. Then blue lines at two locations (33.5°E-119.5°N, 33.5°E-122°N) direct to northeast, while air mass flows back and is elevated to 3500m or higher on 4^{th} February. In contrast, backward trajectories at 6500m height on 4^{th} February (Fig.14b), will take air horizontal and vertical movements into consideration. With sharp decline of low-cloud fraction and unremarkable variation of high-cloud parameters (Fig.16), it can be inferred that the enhanced high-cloud fraction is mainly caused by transmission. In other words, the occurrence of high aerosol layer on 4th February is mainly caused by vertical elevation of air mass from polluted ground and long-distance horizontal transportation from west.

Air mass transportation has great influences on aerosol micro-properties (e.g. particle size, shape, composition) and then clouds development. For example, smoke and polluted dust occur on 1st February (Fig.15) below the height of 3km. There are significant influences on the size distribution and chemical composition of aerosols mixed with dust and polluted particles (Wang et al., 2007; Sun et al., 2010), particularly smoke (Ackerman et al., 2003).The polluted aerosol is likely to be produced by fireworks during the Spring Festival. Additionally, the YRD is an area with significant black carbon (Streets et al., 2001; Bond et al., 2004) and sulfate (Akimoto et al., 1994; Streets et al., 2000; Lu et al., 2010) emissions. Thus, dust particles in this aerosol mass coated with water-soluble materials can easily evolve into CCN. Moreover, an evident increase of cloud amount(Fig.12), is just the same as the results shown by Yu et al. (2007), with a decrease of CDR and an increase of COT appearing in adjacent clouds (low- and mid-low clouds) on the following day (2nd February). These factors amplify the cooling effect at the surface and the top of atmosphere (TOA), consequently, the relatively stable atmosphere appears at low altitude. With the low values of SLI and SLP (Fig.13), large concentrations of $PM_{2.5}$are left on the ground in these two days. Atmosphere suddenly becomes unstable from 3rd February (Fig.13) as AODs and aerosol layer fractions decrease on 2nd February. Also, as shown in Fig.16, from 4th to 7th February, LWPs of low- and mid-low clouds increase systemically from noon to midnight. Under these conditions, with more water vapor and stronger air updraft, it could reduce the critical super-saturation for droplet growth and relatively favor the activation of aerosol particles into CCN, hence, more effectively decreasing the droplet size (Feingold et al., 2003; Kourtidis et al., 2015).

Combined with a relatively comprehensive analysis of meteorological conditions, such as the movement of air mass, sea level pressure and so on, we attempt to use this detailed small case to inform the wider understanding of the overall analysis.

4. Conclusion

The AIE of polluted aerosol over the YRD is analyzed using three-month data (from December 2013 to February 2014) of AODs and cloud parameters from the CERES product. Statistical analyses present that a complex relationship exists between aerosol loadings and micro-/macrophysical parameters of clouds. Aerosol exhibits an important role in complication of cloud evolution in the low layers of troposphere over four typical sub-regions.

The correlations of CDR-AOD, LWP-AOD and COT-AOD tell that despite minor differences in four sub-regions, AIE is in good agreement with Twomey's hypothesis at low-level AODs. With increasing cloud height, the significance level between aerosol and cloud recedes, and AIE mainly stays active at low troposphere (below 5km) in case of the stable atmosphere in wintertime. The ground pollution possibly increase low cloud cover. Synoptic conditions also have significant impact on cloud cover. For instance, the unstable synoptic condition stimulate clouds to develop larger and higher.

In general, meteorological and geographical conditions have strong impact on cloud cover (Norris, 1998). Most studies of AIE do not deliberate that these parameters result in the deviation of cloud quantity and quality. We see more aerosols in plains and valleys at densely populated and industrialized locations, while less aerosols are found in hilly and mountainous regions.

Moreover, airflow brings uncertainty to the assessment of AIE factors based on satellite observation. Further, we need to improve the understanding of physical and thermos-dynamic properties in clouds, which play an important role in cloud development but are not considered in this paper. The classifications of aerosol and clouds are still rough, which cannot accurately illustrate the relationships between aerosol types and different clouds. In addition, a profound interference of geographical factors as well as aerosol climatic impact need further investigation.

Acknowledgements

This research is supported by the National Key Research and Development Program (2016YFC0202003), the National Key Technology R&D Program of Ministry of Science and Technology (2014BAC16B01), and the National Natural Science Foundation of China (41475109, 21577021, 21377028), and partly by the Jiangsu Collaborative Innovation Center for Climate Change.

References

Ackerman, A. S., Toon, O. B., Stevens, D. E., Heymsfield, A. J., Ramanathan, V., &Welton, E. J. (2000). Reduction of tropical cloudiness by soot.*Science*, *288*(5468), 1042-1047.

Ackerman, A. S., Toon, O. B., Stevens, D. E., &Coakley, J. A. (2003). Enhancement of cloud cover and suppression of nocturnal drizzle in stratocumulus polluted by haze. *Geophysical research letters*, *30*(7). http://dx.doi.org/10.1029/2002GL016634.

Akimoto, H., & Narita, H. (1994). Distribution of SO2, NOx and CO2 emissions from fuel combustion and industrial activities in Asia with 1× 1 resolution. *Atmospheric Environment*, *28*(2), 213-225.

Alam, K., Iqbal, M. J., Blaschke, T., Qureshi, S., & Khan, G. (2010). Monitoring spatio-temporal variations in aerosols and aerosol–cloud interactions over Pakistan using MODIS data. *Advances in Space Research*, *46*(9), 1162-1176.

Alam, K., Khan, R., Blaschke, T., &Mukhtiar, A. (2014). Variability of aerosol optical depth and their impact on cloud properties in Pakistan. *Journal of Atmospheric and Solar-Terrestrial Physics*, *107*, 104-112.

Albrecht, B. A. (1989). Aerosols, cloud microphysics, and fractional cloudiness. *Science*, 245, 1227–1230.

Anderson, A. K., &Sobel, N. (2003). Dissociating intensity from valence as sensory inputs to emotion. *Neuron*, *39*(4), 581-583.

Bangert, M., Kottmeier, C., Vogel, B., & Vogel, H. (2011). Regional scale effects of the aerosol cloud interaction simulated with an online coupled comprehensive chemistry model. *Atmospheric Chemistry and Physics*, *11*(9), 4411-4423.

Barnaba, F., &Gobbi, G. P. (2004). Aerosol seasonal variability over the Mediterranean region and relative impact of maritime, continental and Saharan dust particles over the basin from MODIS data in the year 2001.*Atmospheric Chemistry and Physics*, *4*(9/10), 2367-2391.

Bond, T. C., Streets, D. G., Yarber, K. F., Nelson, S. M., Woo, J. H., &Klimont, Z. (2004). A technology ‐ based global inventory of black and organic carbon emissions from combustion. *Journal of Geophysical Research: Atmospheres*, *109*(D14). http://dx.doi.org/10.1029/2003JD003697.

Brenguier, J. L., Pawlowska, H., &Schüller, L. (2003). Cloud microphysical and radiative properties for parameterization and satellite monitoring of the indirect effect of aerosol on climate. *Journal of Geophysical Research: Atmospheres*, *108*(D15). http://dx.doi.org/10.1029/2002JD002682.

Bréon, F. M., Tanré, D., &Generoso, S. (2002). Aerosol effect on cloud droplet size monitored from satellite. *Science*, *295*(5556), 834-838.

Burnet, F.; Brenguier, J.-L. (2007) Observational study of the entrainment-mixing process in warm convective clouds. *J. Atmos. Sci.*, *64*, 1995–

2011.

Chan, C. K., & Yao, X. (2008). Air pollution in mega cities in China. *Atmospheric environment*, *42*(1), 1-42.

Chen, S., Bartello, P., Yau, M. K., Vaillancourt, P. A., & Zwijsen, K. (2016). Cloud Droplet Collisions in Turbulent Environment: Collision Statistics and Parameterization. *Journal of the Atmospheric Sciences*, *73*(2), 621-636.

Costantino, L., &Bréon, F. M. (2013). Aerosol indirect effect on warm clouds over South-East Atlantic, from co-located MODIS and CALIPSO observations. *Atmospheric Chemistry and Physics*, *13*(1), 69-88.

Draxler, R. R., &Rolph, G. D. (2003). HYSPLIT (HYbrid Single-Particle Lagrangian Integrated Trajectory) model access via NOAA ARL READY website (http://www.arl.noaa.gov/ready/hysplit4. html). NOAA Air Resources Laboratory, Silver Spring.

Feingold, G., Eberhard, W. L., Veron, D. E., &Previdi, M. (2003). First measurements of the Twomey indirect effect using ground‐based remote sensors. *Geophysical Research Letters*, *30*(6). http://dx.doi.org/10.1029/2002GL016633.

Ferek, R.; Garrett, T.; Hobbes, P.V.; Strader, S.; Johnson, D.; Taylor, J.; Nielson, K.; Ackerman, A.; Kogan, Y.; Liu, Q.; et al. (2000) Drizzle suppression in ship tracks. *J. Atmos. Sci.*, *57*, 2707–2728.

Forest, C. E., Stone, P. H., Sokolov, A. P., Allen, M. R., & Webster, M. D. (2002). Quantifying uncertainties in climate system properties with the use of recent climate observations. *Science*, *295*(5552), 113-117.

Fu, X., Wang, S. X., Cheng, Z., Xing, J., Zhao, B., Wang, J. D., &Hao, J. M. (2014). Source, transport and impacts of a heavy dust event in the Yangtze River Delta, China, in 2011. *Atmospheric Chemistry and Physics*, 14(3), 1239-1254.

Grandey, B. S., Stier, P., & Wagner, T. M. (2013). Investigating relationships between aerosol optical depth and cloud fraction using satellite, aerosol reanalysis and general circulation model data. *Atmospheric Chemistry and Physics*, *13*(6), 3177-3184.

Gryspeerdt, E., Stier, P., & Partridge, D. G. (2014). Satellite observations of cloud regime development: the role of aerosol processes. *Atmospheric Chemistry and Physics*, *14*(3), 1141-1158.

Hansen, J., Sato, M., &Ruedy, R. (1997). Radiative forcing and climate response. *Journal of Geophysical Research: Atmospheres*, *102*(D6), 6831-6864.

He, Q., Li, C., Geng, F., Lei, Y., & Li, Y. (2012). Study on long-term aerosol distribution over the land of East China using MODIS data. *Aerosol and Air Quality Research*, *12*(3), 304-319.

Hu, Q., Fu, H., Wang, Z., Kong, L., Chen, M., & Chen, J. (2016). The variation of characteristics of individual particles during the haze evolution in the urban Shanghai atmosphere. *Atmospheric Research*, *181*, 95-105.

Jin, M., & Shepherd, J. M. (2008). Aerosol relationships to warm season clouds and rainfall at monthly scales over east China: Urban land versus ocean. *Journal of Geophysical Research: Atmospheres*, *113*(D24). http://dx.doi.org/10.1029/2008JD010276.

Jones, T. A., Christopher, S. A., & Quaas, J. (2009). A six year satellite-based assessment of the regional variations in aerosol indirect effects. *Atmospheric Chemistry and Physics*, *9*(12), 4091-4114.

Kalnay, E., Kanamitsu, M., Kistler, R., Collins, W., Deaven, D., Gandin, L., et al. (1996). The NCEP/NCAR 40-year reanalysis project. *Bulletin of the American meteorological Society*, *77*(3), 437-471.

Karydis, V. A., Kumar, P., Barahona, D., Sokolik, I. N., &Nenes, A. (2011). On the effect of dust particles on global cloud condensation nuclei and cloud droplet number. *Journal of Geophysical Research: Atmospheres*, *116*(D23). http://dx.doi.org/10.1029/2011JD016283.

Knutti, R., Stocker, T. F., Joos, F., &Plattner, G. K. (2002). Constraints on radiative forcing and future climate change from observations and climate model ensembles. *Nature*, *416*(6882), 719-723.

Kong, S., Li, X., Li, L., Yin, Y., Chen, K., Yuan, L., et al. (2015). Variation of polycyclic aromatic hydrocarbons in atmospheric PM 2.5 during winter haze period around 2014 Chinese Spring Festival at Nanjing:

Insights of source changes, air mass direction and firework particle injection. *Science of the Total Environment*, *520*, 59-72.

Koren, I.; Kaufman, Y.J.; Remer, L.A.; Martins, V. (2004) Measurement of the effect of Amazon smoke on inhibition of cloud formation. *Science, 303*, 1342–1345.

Koren, I.; Kaufman, Y.J.; Rosenfeld, D.; Remer, L.A.; Rudich, Y. (2005) Aerosol invigoration and restructuring of Atlantic convective clouds. *Geophys. Res. Lett.*, doi:10.1029/2005GL023187.

Koren, I., Feingold, G., & Remer, L. A. (2010). The invigoration of deep convective clouds over the Atlantic: aerosol effect, meteorology or retrieval artifact?. *Atmospheric Chemistry and Physics*, *10*(18), 8855-8872.

Kourtidis, K., Stathopoulos, S., Georgoulias, A. K., Alexandri, G., &Rapsomanikis, S. (2015). A study of the impact of synoptic weather conditions and water vapor on aerosol–cloud relationships over major urban clusters of China. *Atmospheric Chemistry and Physics*, *15*(19), 10955-10964.

L'Ecuyer, T. S., Berg, W., Haynes, J., Lebsock, M., &Takemura, T. (2009). Global observations of aerosol impacts on precipitation occurrence in warm maritime clouds. *Journal of Geophysical Research: Atmospheres*, *114*(D9). http://dx.doi.org/10.1029/2008JD011273.

Lebsock, M. D., Stephens, G. L., &Kummerow, C. (2008). Multisensor satellite observations of aerosol effects on warm clouds. *Journal of Geophysical Research: Atmospheres*, *113*(D15). http://dx.doi.org/10.1029/2008JD009876.

Leng, C., Zhang, Q., Tao, J., Zhang, H., Zhang, D., Xu, C., et al. (2014). Impacts of new particle formation on aerosol cloud condensation nuclei (CCN) activity in Shanghai: case study. *Atmospheric Chemistry and Physics*, *14*(20), 11353-11365.

Leng, C., Duan, J., Xu, C., Zhang, H., Zhang, Q., Wang, Y., et al. (2015). Insights into a historic severe haze weather in Shanghai: synoptic situation, boundary layer and pollutants. *Atmospheric Chemistry & Physics Discussions*, *15*(22).

Liu, J., Zheng, Y., Li, Z., Flynn, C., &Cribb, M. (2012). Seasonal variations of aerosol optical properties, vertical distribution and associated radiative effects in the Yangtze Delta region of China. *Journal of Geophysical Research: Atmospheres*, *117*(D16). http://dx.doi.org/10.1029/2011JD016490.

Liu, X., & Wang, J. (2010). How important is organic aerosol hygroscopicity to aerosol indirect forcing? *Environmental Research Letters*, *5*(4), 044010.

Loeb, N. G., & Manalo-Smith, N. (2005). Top-of-atmosphere direct radiative effect of aerosols over global oceans from merged CERES and MODIS observations. *Journal of Climate*, *18*(17), 3506-3526.

Lohmann, U., &Feichter, J. (2005). Global indirect aerosol effects: a review. *Atmospheric Chemistry and Physics*, *5*(3), 715-737.

Lu, Z., Streets, D. G., Zhang, Q., Wang, S., Carmichael, G. R., Cheng, Y. F., et al. (2010). Sulfur dioxide emissions in China and sulfur trends in East Asia since 2000. *Atmospheric Chemistry and Physics*, *10*(13), 6311-6331.

Menon, S., Hansen, J., Nazarenko, L., &Luo, Y. (2002). Climate effects of black carbon aerosols in China and India. *Science*, *297*(5590), 2250-2253.

Michibata, T., Kawamoto, K., &Takemura, T. (2014). The effects of aerosols on water cloud microphysics and macrophysics based on satellite-retrieved data over East Asia and the North Pacific. *Atmospheric Chemistry and Physics*, *14*(21), 11935-11948.

Minnis, P., Young, D. F., Sun-Mack, S., Heck, P. W., Doelling, D. R., &Trepte, Q. Z. (2004, February). CERES cloud property retrievals from imagers on TRMM, Terra, and Aqua. In *Remote Sensing* (pp. 37-48). International Society for Optics and Photonics. http://dx.doi.org/10.1117/12.511210.

Monks, P. S., Granier, C., Fuzzi, S., Stohl, A., Williams, M. L., Akimoto, H., et al. (2009). Atmospheric composition change–global and regional air quality. *Atmospheric environment*, *43*(33), 5268-5350.

Myhre, G., Stordal, F., Johnsrud, M., Kaufman, Y. J., Rosenfeld, D., Storelvmo, T., ... & Isaksen, I. S. (2007). Aerosol-cloud interaction inferred from MODIS satellite data and global aerosol models. *Atmospheric Chemistry and Physics*, *7*(12), 3081-3101.

Norris, J. R. (1998). Low cloud type over the ocean from surface observations. Part I: Relationship to surface meteorology and the vertical distribution of temperature and moisture. *Journal of Climate*, *11*(3), 369-382.

Norris, J. R. (1998). Low cloud type over the ocean from surface observations. Part II: Geographical and seasonal variations. *Journal of Climate*, *11*(3), 383-403.

Penner, J. E., Dong, X., & Chen, Y. (2004). Observational evidence of a change in radiative forcing due to the indirect aerosol effect. *Nature*, *427*(6971), 231-234.

Platnick, S., King, M. D., Ackerman, S. A., Menzel, W. P., Baum, B. A., Riédi, J. C., & Frey, R. A. (2003). The MODIS cloud products: Algorithms and examples from Terra. *IEEE Transactions on Geoscience and Remote Sensing*, *41*(2), 459-473.

Pöschl, U. (2005). Atmospheric aerosols: composition, transformation, climate and health effects. *Angewandte Chemie International Edition*, *44*(46), 7520-7540.

Quaas, J., Boucher, O., & Bréon, F. M. (2004). Aerosol indirect effects in POLDER satellite data and the Laboratoire de Météorologie

Dynamique–Zoom (LMDZ) general circulation model. *Journal of Geophysical Research: Atmospheres*, *109*(D8). http://dx.doi.org/10.1029/2003JD004317.

Ramanathan, V., Crutzen, P. J., Lelieveld, J., Mitra, A. P., Althausen, D., Anderson, J., et al. (2001). Indian Ocean Experiment: An integrated analysis of the climate forcing and effects of the great Indo‐Asian haze. *Journal of Geophysical Research: Atmospheres*, *106*(D22), 28371-28398.

Remer, L. A., Kaufman, Y. J., Tanré, D., Mattoo, S., Chu, D. A., Martins, J. V., et al. (2005). The MODIS aerosol algorithm, products, and validation. *Journal of the atmospheric sciences*, *62*(4), 947-973.

Remer, L. A., & Kaufman, Y. J. (2006). Aerosol direct radiative effect at the top of the atmosphere over cloud free ocean derived from four years of MODIS data. *Atmospheric Chemistry and Physics*, *6*(1), 237-253.

Rolph, G. D. (2003). *Real-time Environmental Applications and Display sYstem (READY) Website (http://www.arl.noaa.gov/ready/hysplit4.html). NOAA Air Resources Laboratory, Silver Spring*. Md.

Rosenfeld, D. (2000). Suppression of rain and snow by urban and industrial air pollution. *Science*, *287*(5459), 1793-1796.

Sardina, G., Picano, F., Brandt, L., & Caballero, R. (2015). Continuous growth of droplet size variance due to condensation in turbulent clouds. *Physical review letters*, *115*(18), 184501.

Satheesh, S. K., Moorthy, K. K., Kaufman, Y. J., &Takemura, T. (2006). Aerosol optical depth, physical properties and radiative forcing over the Arabian Sea. *Meteorology and Atmospheric Physics*, *91*(1-4), 45-62.

Sinclair, V.A., Gray, S.L., Belcher, S.E. (2010) Controls on boundary layer ventilation: Boundary layer processes and large-scale dynamics. *J. Geophys. Res.*, doi:10.1029/2009JD012169.

Sorooshian, A., Feingold, G., Lebsock, M. D., Jiang, H., & Stephens, G. L. (2009). On the precipitation susceptibility of clouds to aerosol perturbations. *Geophysical Research Letters*, *36*(13). http://dx.doi.org/10.1029/2009GL038993.

Sorooshian, A., Wang, Z., Feingold, G., &L'Ecuyer, T. S. (2013). A satellite perspective on cloud water to rain water conversion rates and relationships with environmental conditions. *Journal of Geophysical Research: Atmospheres*, *118*(12), 6643-6650.

Streets, D. G., &Waldhoff, S. T. (2000). Present and future emissions of air pollutants in China: SO2, NOx, and CO. *Atmospheric Environment*, *34*(3), 363-374.

Streets, D. G., Gupta, S., Waldhoff, S. T., Wang, M. Q., Bond, T. C., &Yiyun, B. (2001). Black carbon emissions in China. *Atmospheric environment*, *35*(25), 4281-4296.

Sun, Y., Zhuang, G., Huang, K., Li, J., Wang, Q., Wang, Y., et al. (2010). Asian dust over northern China and its impact on the downstream aerosol chemistry in 2004. *Journal of Geophysical Research: Atmospheres*,*115*(D7). http://dx.doi.org/10.1029/2009JD012757.

Tan, C., Zhao, T., Xu, X., Liu, J., Zhang, L., & Tang, L. (2015). Climatic analysis of satellite aerosol data on variations of submicron aerosols over East China. *Atmospheric Environment*, 123, 392-398.

Tang, J., Wang, P., Mickley, L. J., Xia, X., Liao, H., Yue, X., et al. (2014). Positive relationship between liquid cloud droplet effective radius and aerosol optical depth over Eastern China from satellite data. *Atmospheric Environment*, *84*, 244-253.

Taubman, B.A.; Marufu, L.; Vant-Hull, B.; Piety, C.; Doddridge, B.; Dickerson, R.; Li, Z. (2004) Smoke over haze: Aircraft observations of chemical and optical properties and the effects on heating rates and stability. *J. Geophys. Res.*, doi:10.1029/2003JD003898.

Ten Hoeve, J. E., Remer, L. A., & Jacobson, M. Z. (2011). Microphysical and radiative effects of aerosols on warm clouds during the Amazon biomass burning season as observed by MODIS: impacts of water vapor and land cover. *Atmospheric Chemistry and Physics*, *11*(7), 3021-3036.

Twomey, S. (1974). Pollution and the planetary albedo. *Atmospheric Environment (1967)*, *8*(12), 1251-1256.

Wang, Y., Zhuang, G., Tang, A., Zhang, W., Sun, Y., Wang, Z., &An, Z. (2007). The evolution of chemical components of aerosols at five monitoring sites of China during dust storms. *Atmospheric*

Environment, *41*(5), 1091-1106.

Wang, F., Guo, J., Wu, Y., Zhang, X., Deng, M., Li, X., et al. (2014). Satellite observed aerosol-induced variability in warm cloud properties under different meteorological conditions over eastern China. *Atmospheric Environment*, *84*, 122-132.

Wielicki, B. A., Barkstrom, B. R., Harrison, E. F., Lee III, R. B., Louis Smith, G., & Cooper, J. E. (1996). Clouds and the Earth's Radiant Energy System (CERES): An earth observing system experiment. *Bulletin of the American Meteorological Society*, *77*(5), 853-868.

Winker, D. M., Vaughan, M. A., Omar, A., Hu, Y., Powell, K. A., Liu, Z., et al. (2009). Overview of the CALIPSO mission and CALIOP data processing algorithms. *Journal of Atmospheric and Oceanic Technology*,*26*(11), 2310-2323.

Winker, D. M., Pelon, J., CoakleyJr, J. A., Ackerman, S. A., Charlson, R. J., Colarco, P. R., ... &Kubar, T. L. (2010). The CALIPSO mission: A global 3D view of aerosols and clouds. *Bulletin of the American Meteorological Society*, *91*(9), 1211.

Wolf, M. E., &Hidy, G. M. (1997). Aerosols and climate: Anthropogenic emissions and trends for 50 years. *Journal of Geophysical Research: Atmospheres*, *102*(D10), 11113-11121.

Xia, X., Li, Z., Holben, B., Wang, P., Eck, T., Chen, H., et al. (2007).

Aerosol optical properties and radiative effects in the Yangtze Delta region of China. *Journal of Geophysical Research: Atmospheres*, *112*(D22). http://dx.doi.org/10.1029/2007JD008859.

Xin, J., Wang, Y., Li, Z., Wang, P., Hao, W. M., Nordgren, B. L., et al. (2007). Aerosol optical depth (AOD) and Ångström exponent of aerosols observed by the Chinese Sun Hazemeter Network from August 2004 to September 2005. *Journal of Geophysical Research: Atmospheres*, *112*(D5).

Xu, J., Bergin, M. H., Greenwald, R., & Russell, P. B. (2003). Direct aerosol radiative forcing in the Yangtze delta region of China: Observation and model estimation. *Journal of Geophysical Research: Atmospheres*, *108*(D2). http://dx.doi.org/10.1029/2002JD002550.

Yu, H., Fu, R., Dickinson, R. E., Zhang, Y., Chen, M., & Wang, H. (2007). Interannual variability of smoke and warm cloud relationships in the Amazon as inferred from MODIS retrievals. *Remote Sensing of Environment*, *111*(4), 435-449.

Yuan, T., Li, Z., Zhang, R., & Fan, J. (2008). Increase of cloud droplet size with aerosol optical depth: An observation and modeling study. *Journal of Geophysical Research: Atmospheres*, *113*(D4). http://dx.doi.org/10.1029/2007JD008632.

Zhao, C., Tie, X., & Lin, Y. (2006). A possible positive feedback of reduction of precipitation and increase in aerosols over eastern central

China. *Geophysical Research Letters*, *33*(11).

Figure captions:

Fig. 1. Three-month mean aerosol optical depth (AOD) at 0.55μm over the Yangtze River Delta (YRD) from CERES-SYN between December 2013 and February 2014. The major cities in this region and four focused sub-regions (A, B, C, D) are also marked here.

Fig. 2. Cloud optical thickness (COT) averaged over AOD bins for four sub-regions. The area of circle represents sample number in each bin.

Fig. 3. Same as Fig. 2, but for liquid water path (LWP).

Fig. 4. Same as Fig. 2, but for cloud droplet radius (CDR).

Fig. 5. Profiles of total cloud and aerosol frequencies below 10 km derived from cloud/aerosol layer fraction data.

Fig. 6. The cloud droplet radius (CDR) distribution of 3-h mean low-cloud according to AOD and LWP over four sub-regions. Colors present different levels of AOD from 0 to 1.

Fig. 7. Cloud optical thickness (COT) and cloud droplet radius (CDR) averaged over AOD/LWP bins in log-log scale for four sub-regions.

Fig. 8. Frequency of precipitation amount under clean and polluted conditions in four sub-regions. Colors show different precipitation amount (mm). The *a* and *b* in x-coordinate indicate AOD <0.5 and >0.5, respectively.

Fig. 9. CLF-CTP relationships from CERES-SYN daily products in four sub-region. The whole dataset is sorted as low to high polluted atmospheres by AOD at interval of 0.2.

Fig. 10. CTP-CLF relationships from CERES-SYN daily products in four sub-regions. The whole dataset is sorted as low to high polluted atmospheres by AOD at interval of 0.2.

Fig. 11. Spatial distribution of daily mean AOD (0.55μm) over the Yangtze River Delta (YRD) from 26 January to 8 February 2014.

Fig. 12. Profiles of total cloud and aerosol frequencies below 10 km from CALIPSO daily data in the region of(31-36° E, 117-122° N).

Fig. 13. Daily averages of $PM_{2.5}$, surface lifted index (SLI) and sea-level pressure (SLP) in region (31-36°E, 117-122°N) from 27 January to 8 February 2016. The $PM_{2.5}$ data come from the on-line monitoring and analysis platform for air quality in China (http://www.aqistudy.cn), while the SLIand SLP are from NCEP reanalysis data.

Fig.14. Multiple sites of 3-day air mass (a) forward trajectories starting at 150m on 2 February, (b) backward trajectories ending at 6500m on 4 February.Those trajectories were calculated by the NOAA Hybrid SingleParticle Lagrangian Trajectory (HYSPLIT) model.

Fig. 15. Aerosol subtype on 28 Jan., 1 Feb., 4 Feb. and 6 Feb. retrieved from CALIPSO vertical feature data.

Fig. 16. Time series of cloud property parameters (CF, COT, LWP and CDR) from CERES-SYN 3-h data between 27 Jan. to 28 Feb. 2014. Colors represent clouds at different altitudes.

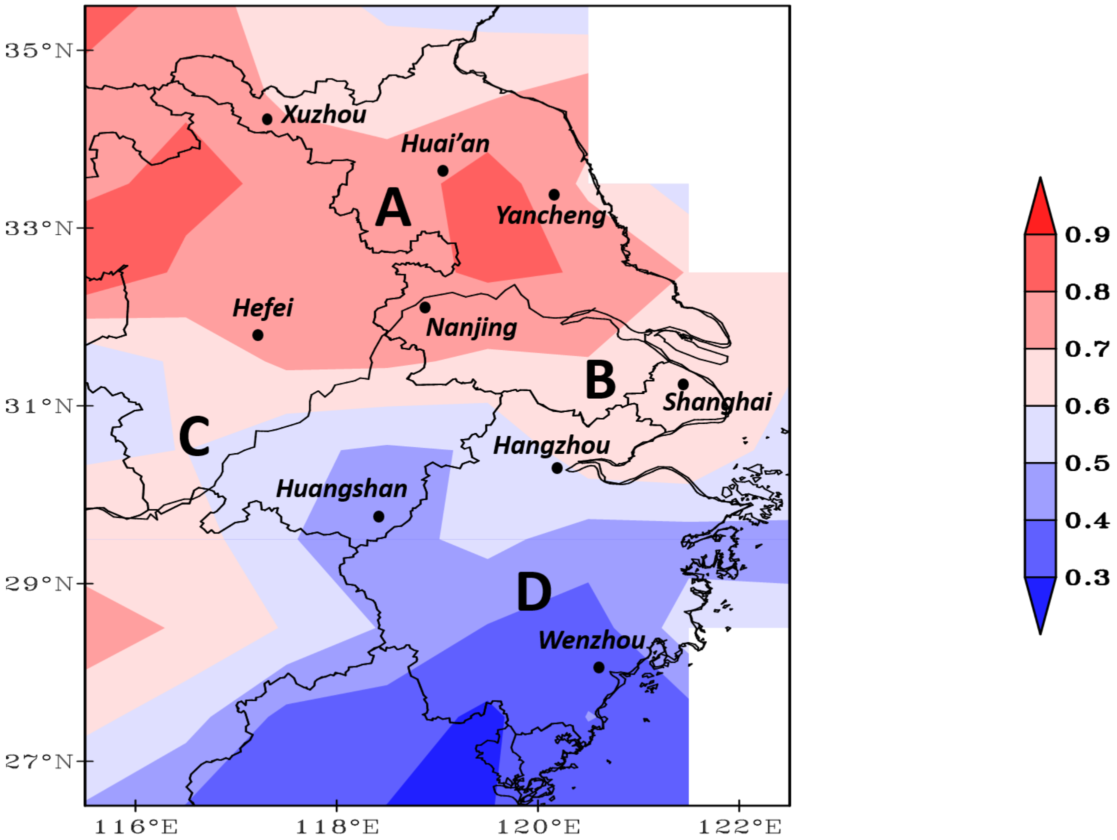

Fig. 1. Three-monthmean aerosol optical depth (AOD) at 0.55μm over the Yangtze River Delta (YRD) from CERES-SYN between December 2013 and February 2014. The major cities in this region and four focused sub-regions (A, B, C, D) are also marked here.

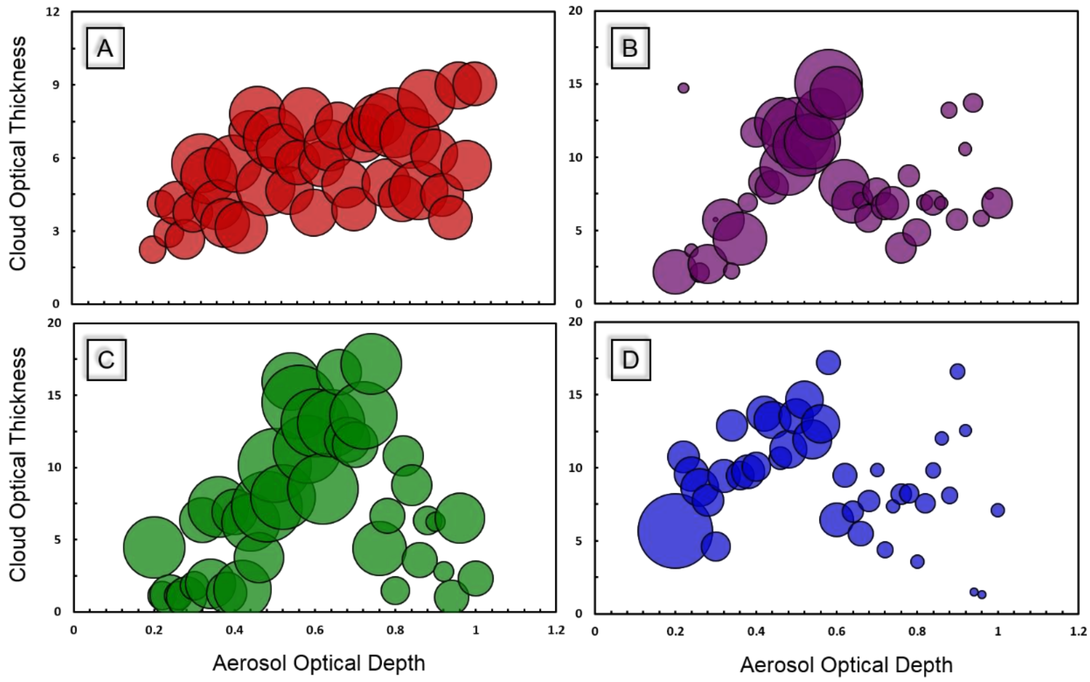

Fig.2. Cloud optical thickness (COT) averaged over AOD bins for four sub-regions. The area of circle represents sample number in each bin.

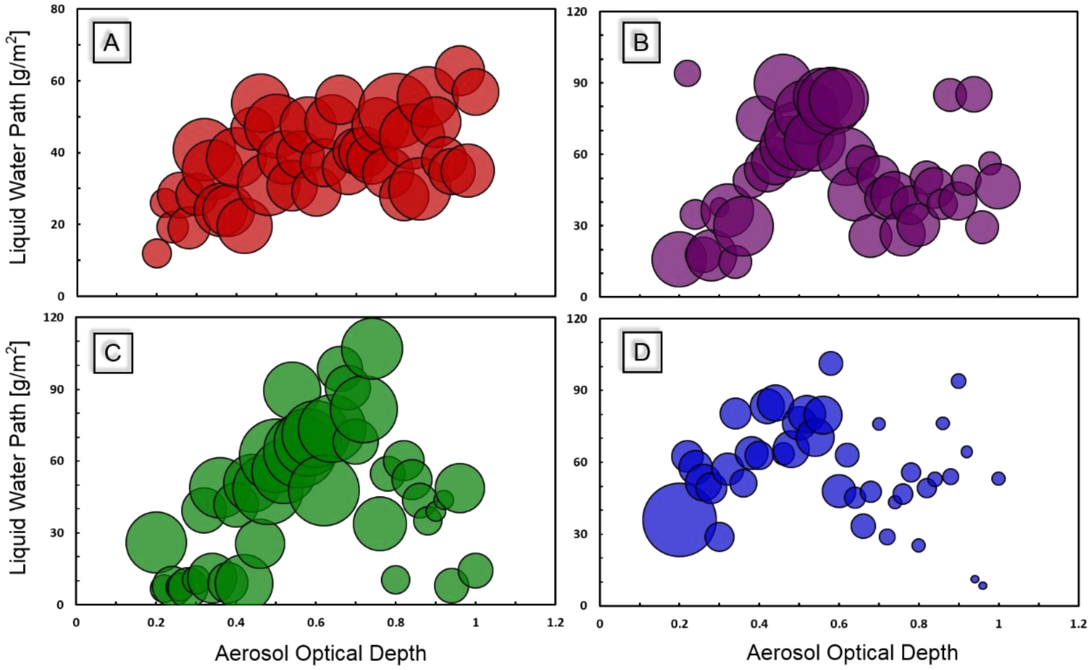

Fig.3. Same as Fig. 2, but for liquid water path (LWP).

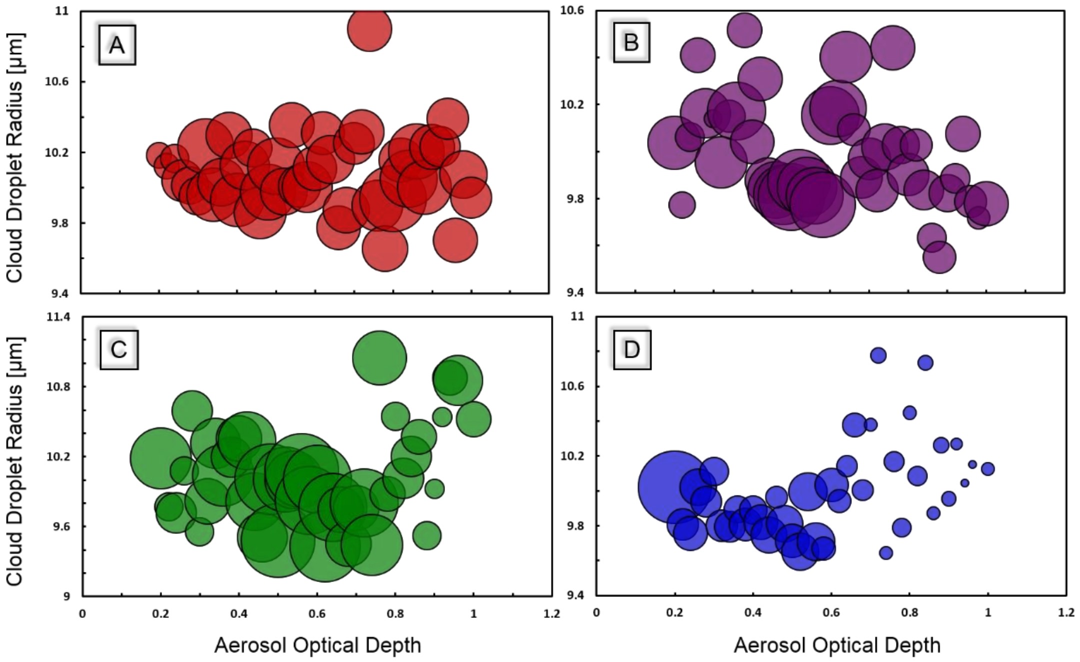

Fig.4. Same as Fig. 2, but for cloud droplet radius (CDR).

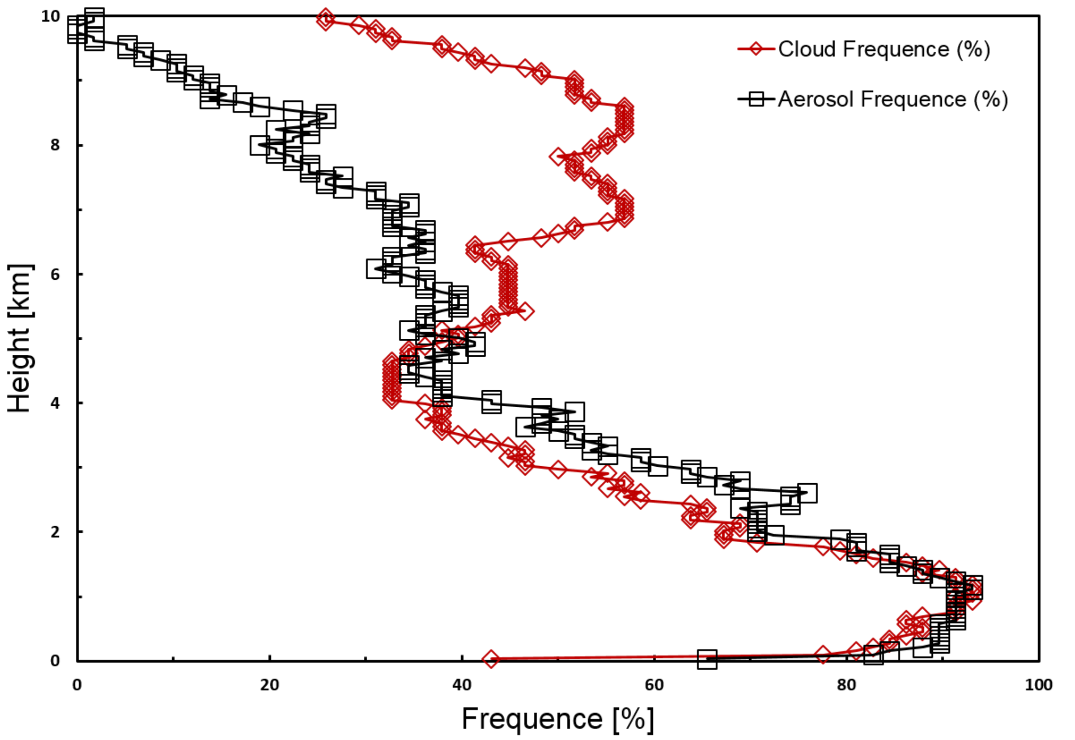

Fig.5. Profiles of total cloud and aerosol frequencies below 10 km derived from cloud/aerosol layer fraction data.

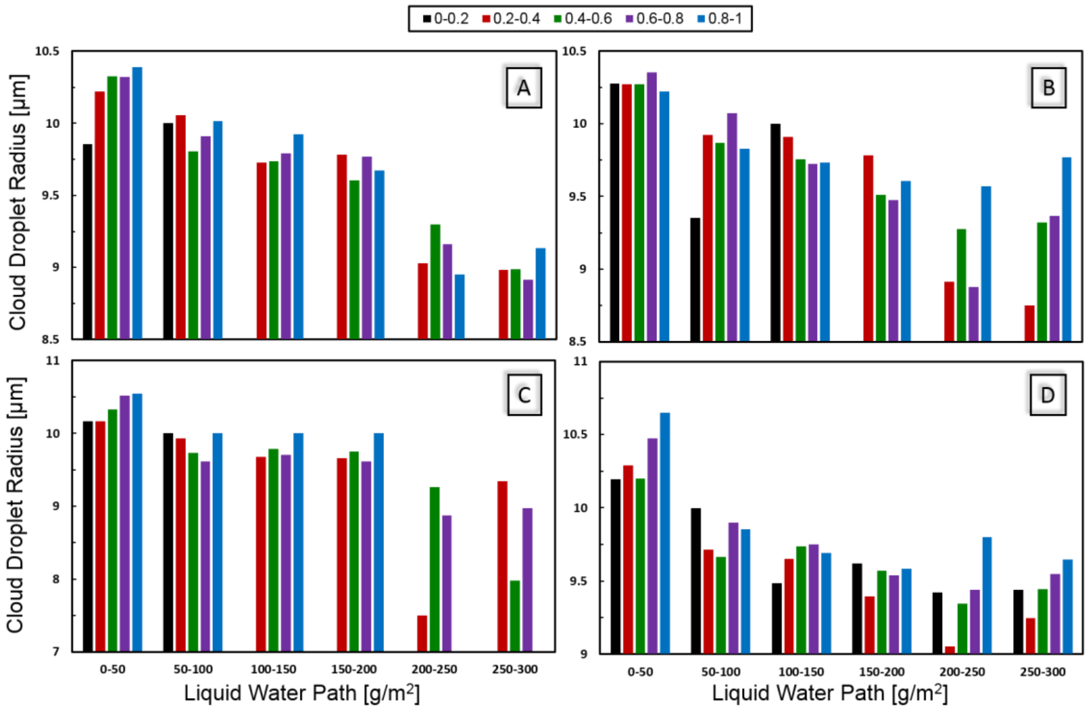

Fig.6. The cloud droplet radius (CDR)distribution of3-h mean low-cloud according to AOD and LWP over four sub-regions. Colors present different levels of AOD from 0 to 1.

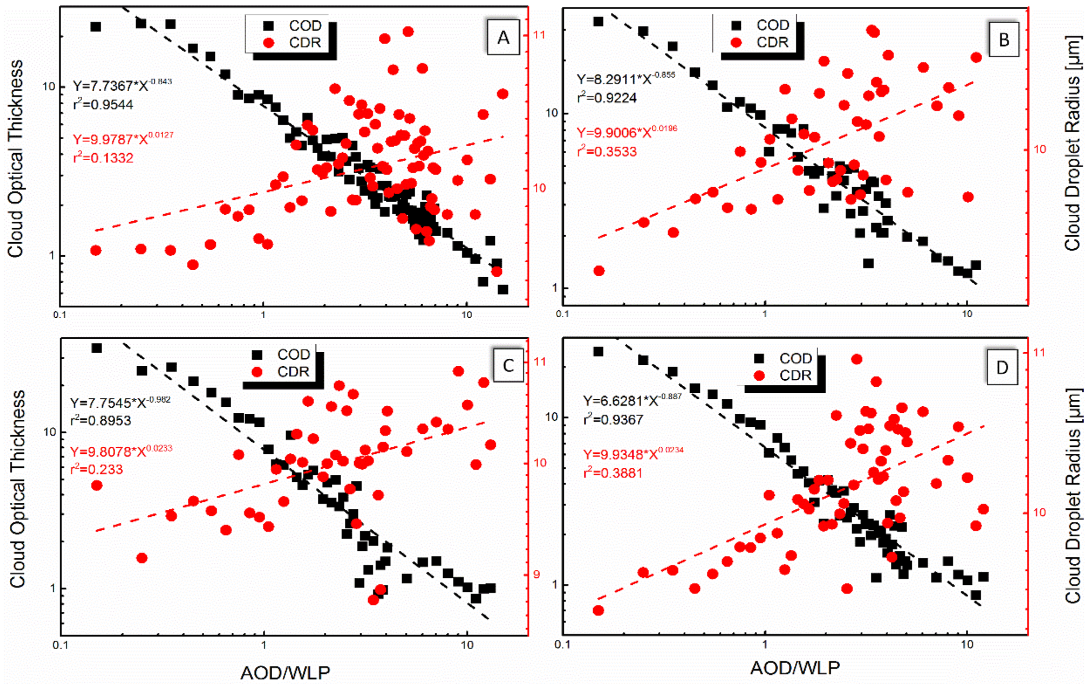

Fig.7. Cloud optical thickness (COT) and cloud droplet radius (CDR) averaged over AOD/LWP bins in log-log scale for four sub-regions.

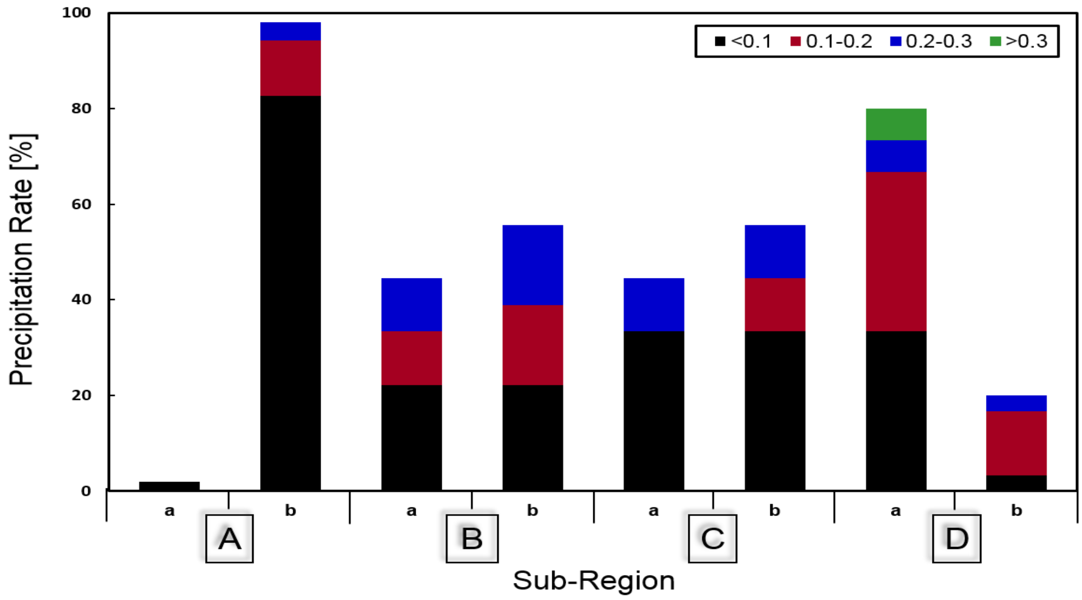

Fig.8. Frequency of precipitation amount under clean and polluted conditions in four sub-regions. Colors show different precipitation amount (mm). The *a* and *b*in x-coordinate indicate AOD<0.5 and >0.5, respectively.

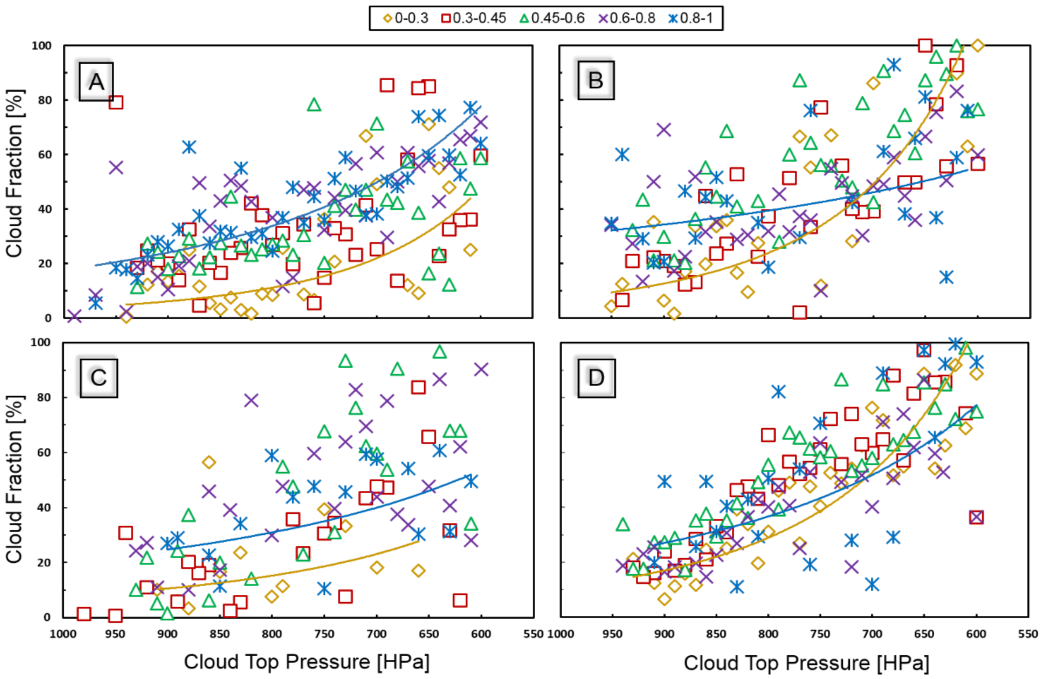

Fig.9. CLF-CTP relationships from CERES-SYN daily products in four sub-region. The whole dataset is sorted as low to high polluted atmospheres by AOD at interval of 0.2.

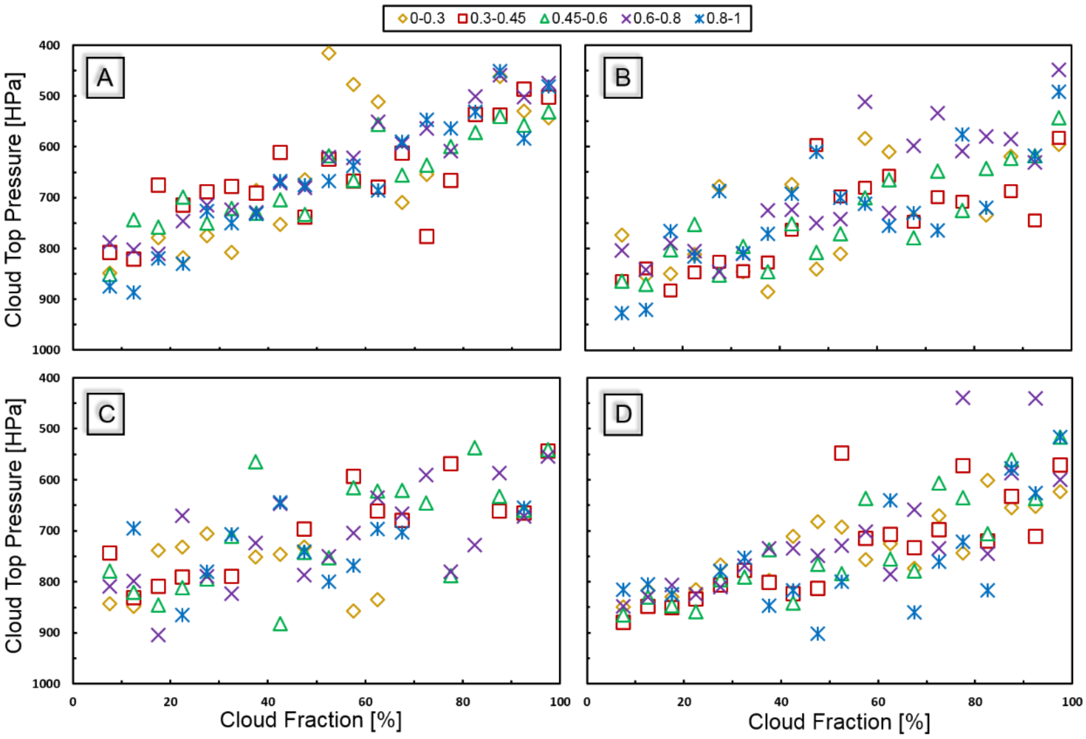

Fig.10. CTP-CLF relationships from CERES-SYN daily products in four sub-regions. The whole dataset is sorted as low to high polluted atmospheresby AOD at interval of 0.2.

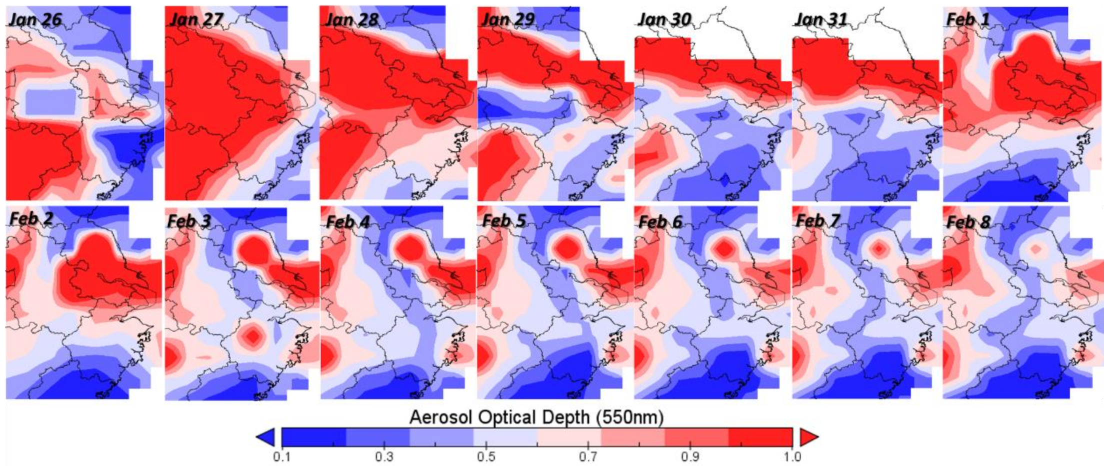

Fig.11. Spatial distribution of daily mean AOD (0.55μm)over the Yangtze River Delta (YRD) from 26 January to 8 February 2014.

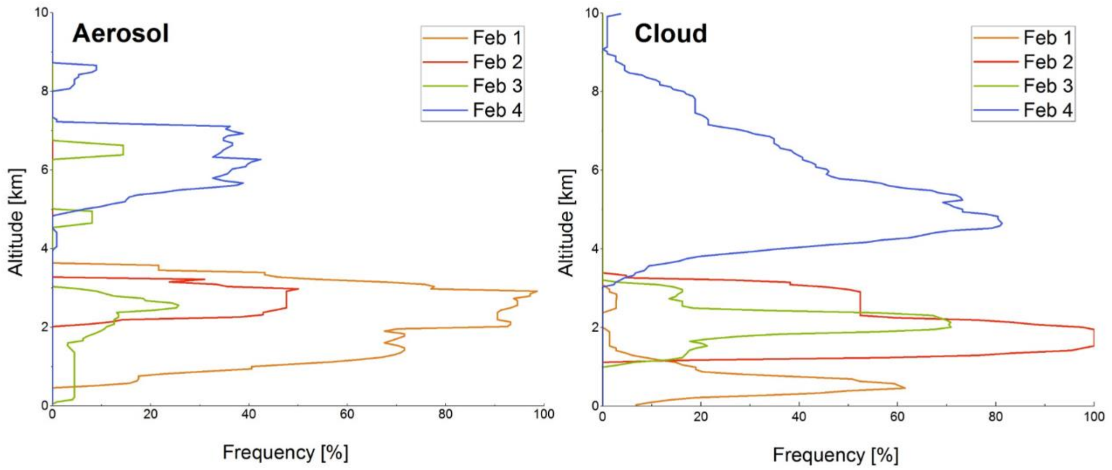

Fig.12. Profiles of total cloud and aerosol frequencies below 10 km from CALIPSO daily data in the region of (31-36°E, 117-122°N).

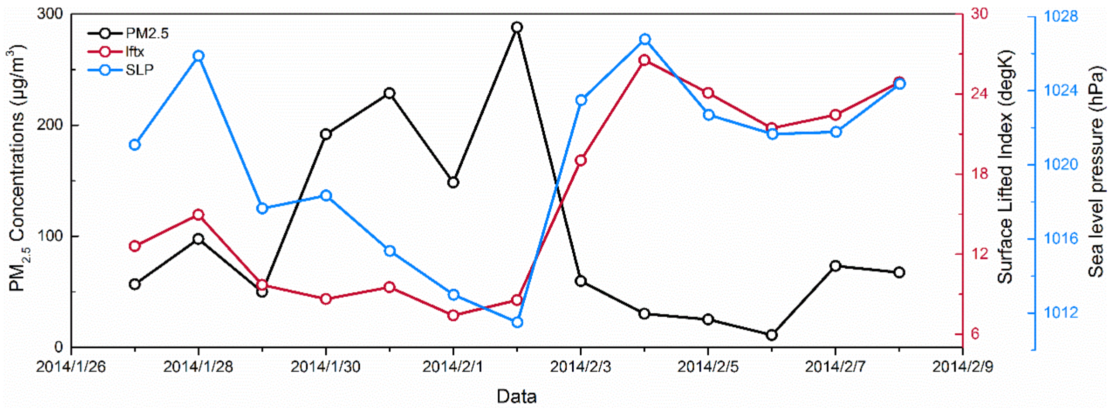

Fig.13. Daily averages of $PM_{2.5}$, surface lifted index (SLI) and sea-level pressure (SLP) in region (31-36°E, 117-122°N) from 27 January to 8 February 2016. The $PM_{2.5}$ data come from the on-line monitoring and analysis platform for air quality in China (http://www.aqistudy.cn), while the SLI and SLP are from NCEP reanalysis data.

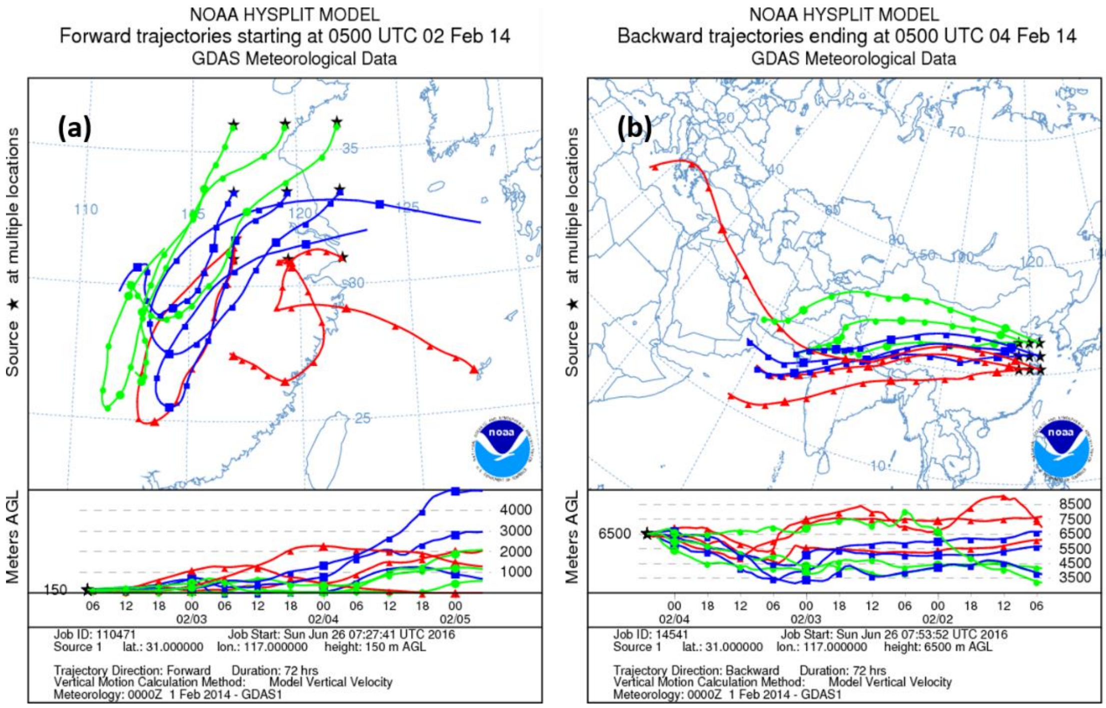

Fig.14. Multiple sites of 3-day air mass (a) forward trajectoriesstarting at 150m on 2 February, (b) backward trajectories ending at 6500m on 4 February. Those trajectories were calculated by the NOAA Hybrid SingleParticle Lagrangian Trajectory (HYSPLIT) model.

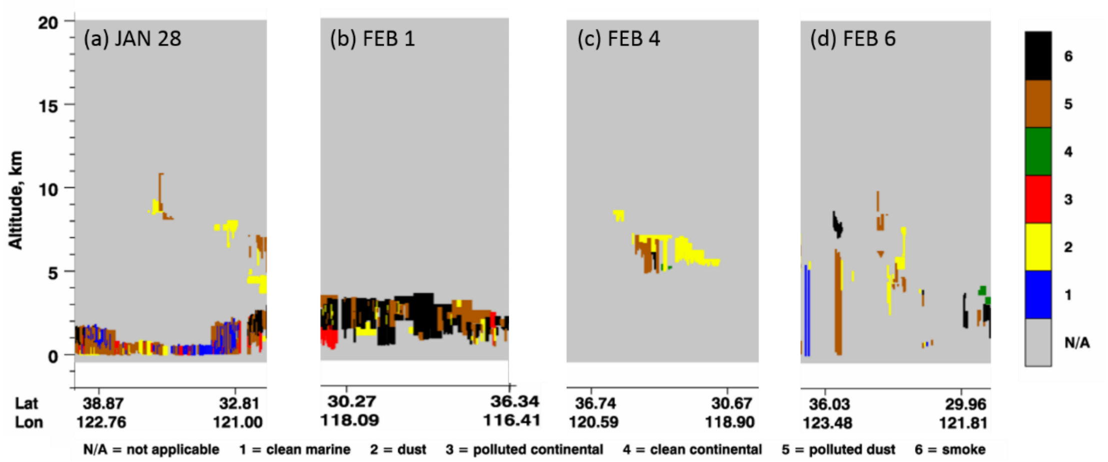

Fig.15. Aerosol subtypeson 28 Jan., 1 Feb., 4 Feb. and 6 Feb. retrieved from CALIPSO vertical feature data.

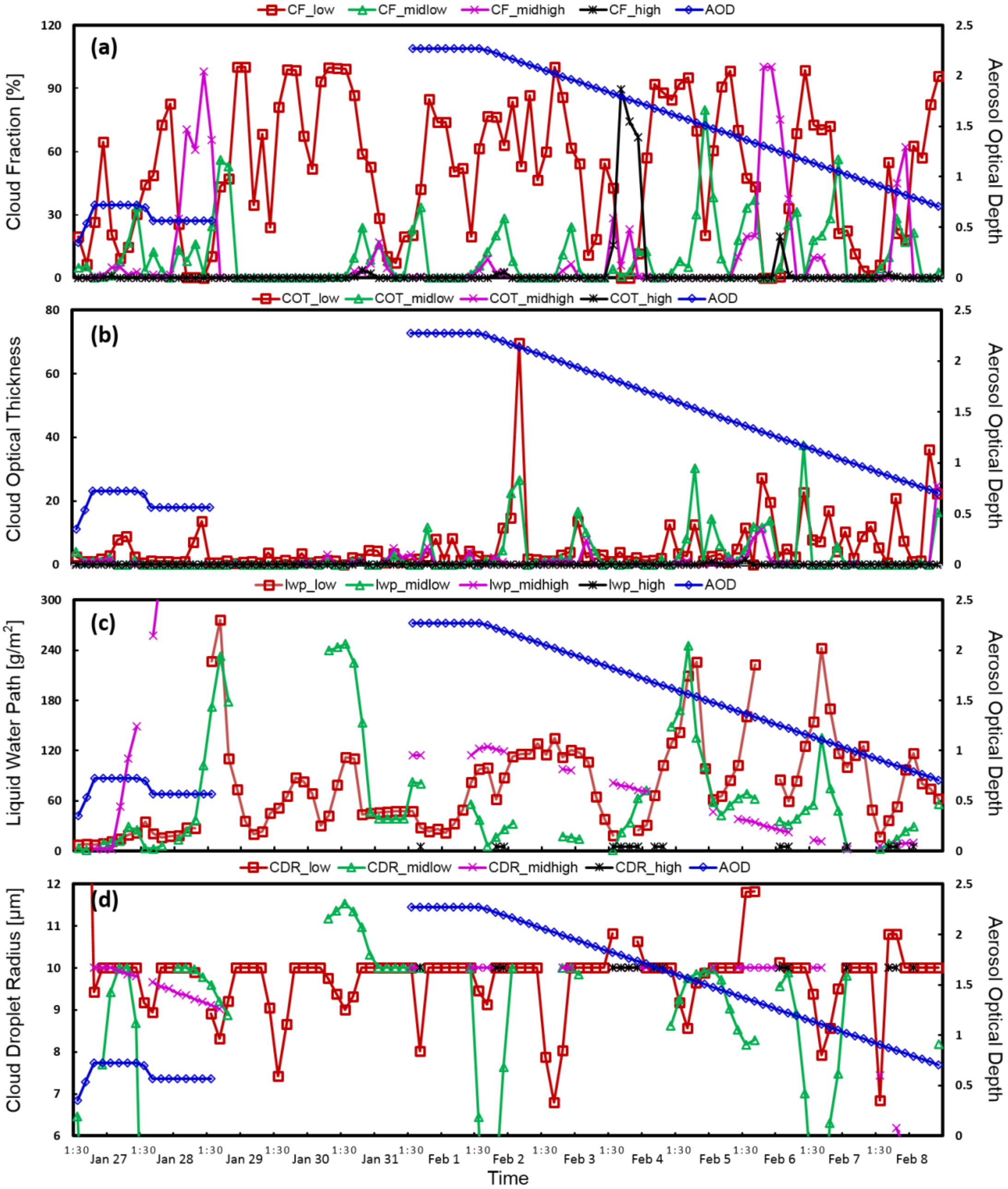

Fig.16. Time series of cloud property parameters (CF, COT, LWP and CDR) from CERES-SYN 3-h data between 27 Jan. to 28 Feb. 2014.Colors representclouds at different altitudes.

Table 1. Details of parameters, which are used in our study.

Parameters	Products	Algorithm & Source	Satellites Channel		Resolution
AOD, FMF	CERES-SYN Edition 3A 3-hour	MODIS-derived (MOD04)	Terra and Aqua	0.55µm	1°×1° (horizontal)
COT, LWP,CTP, CLF, CDR		MODIS-Geostationary (3-hour)-derived		3.7µm (mid-IR)	
Aerosol layer fraction	CAL_LID_L2_05kmAPro-Prov-V3-30	CALIOP lidar-GMAO	CALIPSO		5km (horizontal) 60m (Vertical)
cloud layer fraction					
Aerosol vertical feature mask	CAL_LID_L2_VFM-ValStage1-V3-30				5km (horizontal) 30m (Vertical)
SLI, SLP, precipitation rate	National Center for Environmental Prediction (NCEP) Reanalysis				2.5°×2.5° (horizontal)
Air mass trajectories	HYSPLIT model				Every 6 hours at 9 key sites
$PM_{2.5}$ concentration		Air quality network in China			Daily average

Table 2. AOD-COT, AOD-LWP, AOD-CDR relationships from MODIS daily products of low-cloud in four sub-regions (K is best-fit slope). The whole dataset is sorted as aerosol types based on combined AOD and FMF retrievals.

		Marine aerosol		Dust aerosol		Continental aerosol	
		K	R^2	K	R^2	K	R^2
COT	A	0.1369	0.0034	0.737	0.2978	0.159	0.0101
	B	0.6997	0.4683	0.2815	0.0395	0.444	0.143
	C	1.9429	0.6261	0.4079	0.0211	1.4507	0.4518
	D	1.4804	0.5924	0.2767	0.0478	0.9948	0.2586
LWP	A	0.1754	0.0055	0.6547	0.261	-0.028	0.0004
	B	0.622	0.4233	0.1304	0.0101	0.3177	0.0912
	C	1.9564	0.6332	0.494	0.037	1.3061	0.4106
	D	1.4118	0.5847	0.223	0.0386	0.8059	0.2114
CDR	A	0.0744	0.1846	0.0392	0.1896	-0.039	0.1348
	B	-0.011	0.0113	0.0129	0.038	-0.027	0.0587
	C	0.0109	0.0248	0.0688	0.0969	0.0108	0.0049
	D	0.0232	0.1116	0.0481	0.1599	-0.007	0.0058